Scientific Research Publishing

Advances in Materials Physics and Chemistry, 2022, 12, 177-193
https://www.scirp.org/journal/ampc
ISSN Online: 2162-5328
ISSN Print: 2162-531X

Study of the Composition of a Plasma of Dry Air Contaminated by Al_2O_3, CO, Fe_2O_3 and SiO_2

Yaguibou W. Charles[1,2], Korsaga Eric[1], Korbeogo Aly Rachid[1,3], Koalaga Zacharie[1], Zougmore François[1]

[1]LAME, Université Joseph Ki-Zerbo, Ouagadougou, Burkina Faso
[2]Centre universitaire de Dori, Université Thomas Sankara, Ouagadougou, Burkina Faso
[3]Ecole Polytechnique de Ouagadougou, Ouagadougou, Burkina Faso
Email: weparicharles@gmail.com

How to cite this paper: Charles, Y.W., Eric, K., Rachid, K.A., Zacharie, K. and François, Z. (2022) Study of the Composition of a Plasma of Dry Air Contaminated by Al_2O_3, CO, Fe_2O_3 and SiO_2. *Advances in Materials Physics and Chemistry*, **12**, 177-193.
https://doi.org/10.4236/ampc.2022.128013

Received: April 15, 2022
Accepted: August 27, 2022
Published: August 30, 2022

Abstract

This paper concerns the calculation of equilibrium composition of plasma mixture Air Fe_2O_3, SiO_2, Al_2O_3 and CO in temperatures range 1000 K to 6000 K. We supposed that the plasma is at atmospheric pressure and at local thermodynamic equilibrium (ETL). In the Saharan zone, the aerosols are proven from desert dust and biomass fires. They are essentially composed of oxides of silicon, calcium, iron, aluminum and carbonaceous elements from biomass. Thus, air circuit breakers often operate in a polluted environment without specific protection. They can have abnormal behaviors and failures of cuts. We used Gibbs free energy minimization method to access the different numerical densities of chemical species as a function of temperature. These data are very important to calculate thermodynamic properties, transport coefficients and modeling electrical arc in circuit breakers. The results show that the dust brings many particles which have low dissociation and ionization energies. This leads to an increase in metallic elements and a strong increase in the numerical density of electrons which could have a detrimental effect during the current cut-off phase with the increase in the electrical conductivity of the plasma.

Keywords

Plasma, Aerosol, Equilibrium Composition, Gibbs Free Energy, Arc, Circuit Breaker

1. Introduction

West Africa is dominated by desert aerosols and biomass fires. In recent years, it has suffered from overexploitation of the soil resulting in a reduction in plant

cover and an increase of 30% to 50% in desert dust emissions.

Studies in this sub-region have shown that the chemical composition of aerosols in West Africa is mainly dominated by oxides of silicon, calcium, aluminum, and iron [1]-[9]. In addition, carbonaceous aerosols are produced from biomass and human activities [10] [11] [12] [13]. The collection of aerosols is generally performed on filters by aspiration of a volume of air measured by a sensor (the data are expressed in $\mu g \cdot m^{-3}$) and the chemical composition is determined by spectrometric analysis.

The process of lifting aerosols is a threshold phenomenon which depends essentially on the nature of the soil and the force of the wind direction. The threshold of rising desert aerosols is estimated between 6 $m \cdot s^{-1}$ and 20 $m \cdot s^{-1}$ depending on the nature of the soil. Once injected into the atmosphere, the particles are transported over great distances and form the body of sandstorms. In the case of West Africa, the meeting between the monsoon flow and the harmattan flow favors the high-altitude transport of aerosols: as the harmattan is less dense, it passes over the monsoon and promotes the high-altitude transport of desert aerosols in the rainy season. However, in the dry season, harmattan is the main wind blowing over almost all of West Africa. It continuously causes dust clouds to move [14] [15] [16] [17]. Aerosols are deposited mainly in two ways: dry deposition by sedimentation under the action of gravity and wet deposition by rain.

West African countries like Burkina Faso, therefore, have atmospheres continuously polluted by aerosols. Electrical devices, particularly air circuit breakers, are generally immersed in a dusty atmosphere and operate without specific protection and without maintenance. Aerosols can enter the circuit breaker through the vent holes, settle and form a more or less thick layer on the gasifier cheeks [18]. The medium will therefore contain, in addition to the air composed mainly of nitrogen and oxygen, other chemical elements induced by the aerosols which will modify the composition of the plasma in the circuit breaker during the interruption of the electric current.

This can result in abnormal behavior and failed power cuts of air circuit breakers during their operation [18]. The objective of this work is to show the influence of aerosols on the chemical composition of the air plasma at local thermodynamic equilibrium (ETL) and at atmospheric pressure (1 bar), in a temperature range from 1000 K to 6000 K. We will describe the chosen calculation method, present the results obtained and analyze them.

2. Calculation Method

The study is made at atmospheric pressure. We decided to take into account only the gas phase. We therefore take a temperature range from 1000 K to 6000 K. Several methods are used to determine the composition of plasma: we can quote the law of mass action, the pseudo-kinetic method, the collisional-radiative method, the minimization of the free enthalpy. In this study, we used Gibbs' free

energy minimization method to calculate the composition of plasma at local thermodynamic equilibrium and atmospheric pressure (1 bar). This method was compiled on Matlab software. The Gibbs' free energy minimization method is very efficient and adapted to the type of plasma studied because it only takes into account the chemical nature of the species present in the mixture but not the reaction scheme that can describe the evolution of the mixture.

For air, Fe_2O_3, SiO_2, Al_2O_3 and CO mixtures, we consider the following:

31 monatomic species: C, O, N, Si, Al, Fe, C^+, O^+, N^+, Si^+, Al^+, Fe^+, C^-, O^-, N^-, Si^-, Al^-, Fe^-, C^{2+}, O^{2+}, N^{2+}, Si^{2+}, Al^{2+}, Fe^{2+}, C^{3+}, O^{3+}, N^{3+}, Si^{3+}, Al^{3+}, Fe^{3+}, and electrons;

28 diatomic species: C_2, O_2, N_2, Si_2, Al_2, Fe_2, CO, CN, SiC, AlC, NO, SiO, AlO, SiN, FeO, AlN, C_2^+, O_2^+, N_2^+, CO^+, CN^+, NO^+, AlO^+, N_2^-, C_2^-, O_2^-, CN^- and AlO^-;

40 polyatomic species: CO_2, C_3, CCN, CNC, CNN, C_2O, O_3, N_3, NCO, NO_2, N_2O, NCN, SiC_2, SiO_2, Si_2C, Si_2N, Si_3, AlC_2, AlO_2, Al_2O, OCCN, C_2N_2, CNCOCN, C_3O_2, C_4, NO_3, N_2O_3, N_2O_4, N_2O_5, Al_2C_2, Al_2O_2, Al_2O_3, $Fe(CO)_5$, N_2O^+, CO_2^+, Al_2O^+, $Al_2O_2^+$, AlO_2^-, NO_3^-, NO_2^-

We decided to only take into account the gas phase. We consider that plasma contains eigthy eigth ($N = 99$) chemical species. Determining the composition at equilibrium requires prior knowledge of the specific chemical potentials of all the particles inhabiting the plasma [19].

For electrons, atomic species and molecules, their chemical potential can be determined using specific enthalpy and specific entropy data tabulated by National Institute of Standards and Technology (NIST), Bonnie and Bendjebbar [20] [21] [22] [23]. We mainly use the thermodynamic data tabulated by Bonnie in the calculation of specific thermodynamic properties. The specific heat capacity, the specific enthalpy and the specific entropy are obtained by the following relations [22]:

$$\frac{C_p^0(T)}{R} = a_1T^{-2} + a_2T^{-1} + a_3 + a_4T + a_5T^2 + a_6T^3 + a_7T^4 \tag{1}$$

$$\frac{H^0(T)}{RT} = -a_1T^{-2} + \frac{a_2\ln(T)}{T} + a_3 + \frac{a_4T}{2} + \frac{a_5T^2}{3} + \frac{a_6T^3}{4} + \frac{a_7T^4}{5} + \frac{b_1}{T} \tag{2}$$

$$\frac{S^0(T)}{R} = -\frac{a_1T^{-2}}{2} - a_2T^{-1} + a_3\ln(T) + a_4T + \frac{a_5T^2}{2} + \frac{a_6T^3}{3} + \frac{a_7T^4}{4} + b_2 \tag{3}$$

R is the ideal gas constant and T the temperature in Kelvin.

Thus the chemical potential as a function of the temperature is given by the following formula:

$$\mu^0 = H^0 - TS^0 \tag{4}$$

To determine the concentrations of different chemical species, we use Gibbs' free energy minimization calculation method [24]-[31]. We first determine the numbers of moles and from these one we calculate the concentrations.

Let $Y(y_1, y_2, \cdots, y_n)$ be the number of moles of species. The numbers of

moles must satisfy the electric neutrality and the conservation of the number of nuclei in the plasma. These conditions are obtained by:

$$\sum a_{ij} y_i = b_j \quad (j = 1, 2, \cdots, m) \tag{5}$$

In this equation, N is the number of chemical species; m is the number of types of nuclei in the mixture including electrons; a_{ij} the number of j type nucleus in molecule i (the a_{ij} corresponds to the coefficients of the decomposition matrix of the different species) and b_j represents the number of initial j type nuclei.

We have seven different types of nuclei in our plasma (e^-, C, O, N, Si, Al, Fe) so $m = 7$. $b_j = 0$ reflects the electric neutrality in the electric arc plasma. The Gibbs free energy for plasmas at several temperatures is given by the following equation [24] [32]:

$$E(Y) = \sum_{i=1}^{N} y_i \left(\mu_i^0 + RT_i \ln\left(\frac{P}{P_0}\right) + RT_i \ln\left(\frac{y_i T_i}{\sum_{k=1}^{N} y_k T_k}\right)\right) \tag{6}$$

P_0 is the reference pressure (P_0 = 1E5 Pa) and P the pressure at a given temperature; T_i is the translation temperature of particle i.

A simplified expression of Equation (6) is given by:

$$E(Y) = \sum_{i=1}^{N} y_i \left(C_i + RT_i \ln\left(\frac{y_i T_i}{\sum_{k=1}^{N} y_k T_k}\right)\right) \tag{7}$$

with

$$C_i = \mu_i^0 + RT_i \ln\left(\frac{P}{P_0}\right) \tag{8}$$

The y_i are the numbers of moles. We must find the point $Y(y_1, y_2, \cdots, y_n)$ which minimizes the function E (Y) and for which the coordinates y_i satisfy the following conditions:

- the mole numbers must be positive $y_i \geq 0 \quad \forall i$;
- the coordinates y_i must satisfy the conservation of the number of nuclei and the electric-neutrality.

After a Taylor series expansion of order 2 around point $Y(y_1, y_2, \cdots, y_n)$, we get:

$$Q(X) = E(Y) + \sum_{i=1}^{N} \left(\frac{\partial E}{\partial x_i}\right)_{X=Y} (x_i - y_i) + \frac{1}{2} \sum_{i=1}^{N} \sum_{k=1}^{N} \left(\frac{\partial^2 E}{\partial x_i \partial y_k}\right)_{X=Y} (x_i - y_i)(x_k - y_k) \tag{9}$$

Which leads to:

$$Q(X) = E(Y) + \sum_{i=1}^{N} (x_i - y_i) \left(C_i + RT_i \ln\left(\frac{y_i T_i}{\sum_{k=1}^{N} y_k T_k}\right)\right) + \frac{1}{2} \left(\sum_{i=1}^{N} y_i RT_i \left(\frac{x_i - y_i}{y_i} - \frac{\sum_k (x_k - y_k)}{\sum_{k=1}^{N} y_k T_k}\right)\right) \tag{10}$$

Taking into account the physical conditions (Equation (5)), we introduce the Lagrange multipliers π_i. Thus, we get the function $\xi(X)$.

$$\xi(X) = Q(X) + \sum_j \pi_j \left(-\sum a_{ij} x_i + b_j \right) \tag{11}$$

$E(X)$ is minimum when [33] $\dfrac{\partial \xi(X)}{\partial x_i} = 0$

Which leads to:

$$\frac{f_i}{y_i} = RT_i \left[\frac{x_i}{y_i} - \frac{\sum_k T_k x_k}{\sum_k T_k y_k} \right] - \sum_{i=1}^{m} a_{ij} = 0 \tag{12}$$

with

$$f_i = y_i \left(C_i + RT_i \ln \left(\frac{y_i T_i}{\sum_{k=1}^{N} y_k T_k} \right) \right) \tag{13}$$

Using the Newton-Raphson method, we obtain a system of equations [21] [23] [34]:

$$\begin{pmatrix} \frac{RT_1}{y_1} & \cdots & 0 & a_{11} & \cdots & a_{1m} \\ \vdots & \ddots & \vdots & \vdots & \ddots & \vdots \\ 0 & \cdots & \frac{RT_N}{y_N} & a_{N1} & \cdots & a_{Nm} \\ a_{11} & \cdots & a_{1m} & 0 & \cdots & 0 \\ \vdots & \ddots & \vdots & \vdots & \ddots & \vdots \\ a_{N1} & \cdots & a_{Nm} & 0 & \cdots & 0 \end{pmatrix}$$

$$= \begin{pmatrix} -\mu_1^0 - RT_1 \ln \left(\frac{T_1 y_1}{\sum_{k=1}^{N} y_k T_k} \right) - RT_1 \ln \left(\frac{P}{P_0} \right) - \sum_{j=1}^{m} \pi_j a_{ij} \\ \vdots \\ -\mu_N^0 - RT_N \ln \left(\frac{T_N y_N}{\sum_{k=1}^{N} y_k T_k} \right) - RT_N \ln \left(\frac{P}{P_0} \right) - \sum_{j=1}^{m} \pi_j a_{ij} \\ -\sum_{j=1}^{m} y_i a_{i1} + b_1 \\ \vdots \\ -\sum_{j=1}^{m} y_i a_{im} + b_m \end{pmatrix} \tag{14}$$

In the case of our study, we took into account ninety-ninie (99) chemical species, so $N = 99$. The Equation (14) is therefore a system of 106 equations with 103 unknowns, which are the number of moles of the 99 chemical species and

seven (7) Lagrange multipliers. The temperature of the medium was maintained at $T_i = T$. The principle of this numerical method consists of initially and arbitrarily assigning values to the number of moles $i \in [1,99]$ and the Lagrange multipliers $j \in [1,7]$. The number of moles must satisfy Condition (5).

The new values of the number of moles (n_i) and Lagrange multipliers (π_j) were obtained by solving Equation (14). This leads to the following system.

$$\begin{cases} n_i = y_i + \lambda \Delta n_i & \forall i \in [\![1, N = 99]\!] \\ \pi_j = \pi_j + \lambda \Delta \pi_j & \forall j \in [\![1, m = 7]\!] \end{cases} \tag{15}$$

The parameter $\lambda \in [0,1]$ is the correction coefficient. This helps to avoid negative values of the mole numbers that may appear when moving away from the solution. It must satisfy the condition of $\frac{\mathrm{d}E(\lambda)}{\mathrm{d}\lambda} \prec 0$ to avoid going beyond the point of convergence. This corresponded to the largest value between 0 and 1.

$$n_i = y_i + \lambda \Delta n_i \succ 0 \quad \forall i \in [\![1, N]\!] \tag{16}$$

The new values of the number of moles and Lagrange multipliers were used for a new calculation cycle. The criterion for interrupting iterations was set by the following condition given by Cayet [33]:

$$\frac{G(n_i) - G(y_i)}{G(n_i)} \prec 10^{-14} \tag{17}$$

The numerical densities (x_i) were obtained using Dalton's law [24].

$$X_i = n_i \frac{\frac{P - \Delta P}{k}}{T \sum_i^N n_i} \tag{18}$$

k is the Boltzmann constant and ΔP is the lowering of the pressure given by the following equation:

$$\Delta P = -\frac{kT}{24\pi\lambda_d^3} \tag{19}$$

λ_d the Debye length is given by Equation (20):

$$\lambda_d = \frac{1}{N_A e}\left(\sum_{i=1}^{N} \frac{\varepsilon_0 RT}{x_e}\right)^{1/2} \tag{20}$$

where ε_0 is the permittivity of vacuum, x_e is the mole fraction of electrons, e is the elementary charge, and N_A Avogadro's number.

Tables 1-3 present the thermodynamics data coefficients using in the calculation of equilibrium composition.

3. Results

In this section, we present the composition of the dry air plasma of an air circuit breaker operating under normal conditions and the compositions of the air

plasmas of an air circuit breaker that can be contaminated by aerosols. The study was conducted at local thermodynamic equilibrium.

Table 1. Thermodynamic data coefficients (a).

Particles	a_1	a_2	a_3	a_4	a_5	a_6	a_7	b_1	b_2
e^-	0.00E+00	0.00E+00	2.50E+00	0.00E+00	0.00E+00	0.00E+00	0.00E+00	−7.45E+02	−1.17E+01
C	−1.29E+05	1.72E+02	2.65E+00	−3.35E−04	1.74E−07	−2.90E−11	1.64E−15	8.41E+04	4.13E+00
O	2.62E+05	−7.30E+02	3.32E+00	−4.28E−04	1.04E−07	−9.44E−12	2.73E−16	3.39E+04	−6.68E−01
N	8.88E+04	−1.07E+02	2.36E+00	2.92E−04	−1.73E−07	4.01E−11	−2.68E−15	5.70E+04	4.87E+00
Si	−6.17E+05	2.24E+03	−4.45E−01	1.71E−03	−4.11E−07	4.56E−11	−1.89E−15	3.95E+04	2.68E+01
Al	−2.92E+04	1.17E+02	2.36E+00	7.74E−05	−1.53E−08	−9.97E−13	5.05E−16	3.82E+04	6.60E+00
Fe	−1.95E+06	6.74E+03	−5.49E+00	4.38E−03	−1.12E−06	1.54E−10	−8.02E−15	7.14E+03	6.50E+01
C_2	−9.69E+05	3.56E+03	−5.06E−01	2.95E−03	−7.14E−07	8.67E−11	−4.08E−15	7.68E+04	3.34E+01
O_2	−1.04E+06	2.34E+03	1.82E+00	1.27E−03	−2.19E−07	2.05E−11	−8.19E−16	−1.69E+04	1.74E+01
N_2	5.88E+05	−2.24E+03	6.07E+00	−6.14E−04	1.49E−07	−1.92E−11	1.06E−15	1.28E+04	−1.59E+01
Si_2	1.37E+06	−4.21E+03	9.34E+00	−2.75E−03	9.59E−07	−1.37E−10	6.77E−15	9.51E+04	−3.17E+01
Al_2	−2.32E+06	9.22E+03	−9.45E+00	1.00E−02	−3.15E−06	4.36E−10	−2.24E−14	2.90E+03	9.96E+01
CN	−2.23E+06	5.04E+03	−2.12E−01	1.35E−03	1.33E−07	−6.94E−11	5.49E−15	1.78E+04	3.28E+01
CO	4.62E+05	−1.94E+03	5.92E+00	−5.66E−04	1.40E−07	−1.79E−11	9.62E−16	−2.47E+03	−1.39E+01
NO	2.24E+05	−1.29E+03	5.43E+00	−3.66E−04	9.88E−08	−1.42E−11	9.38E−16	1.75E+04	−8.50E+00
SiC	−6.27E+04	7.21E+02	2.16E+00	2.20E−03	−6.57E−07	9.18E−11	−4.97E−15	8.32E+04	1.60E+01
SiN	−2.93E+06	5.85E+03	1.32E+00	1.26E−03	−3.77E−07	6.89E−11	−4.19E−15	6.53E+03	2.55E+01
SiO	−1.77E+05	−3.20E+01	4.48E+00	4.59E−06	3.56E−08	−1.33E−11	1.61E−15	−1.35E+04	−8.39E−01
AlC	1.94E+06	−6.75E+03	1.35E+01	−5.85E−03	1.93E−06	−2.59E−10	1.22E−14	1.23E+05	−6.15E+01
AlN	3.82E+06	−1.07E+04	1.45E+01	−3.73E−03	7.92E−07	−8.09E−11	2.89E−15	1.21E+05	−7.29E+01
AlO	1.57E+04	3.86E+03	−5.93E+00	9.05E−03	−2.93E−06	4.24E−10	−2.28E−14	−1.33E+04	6.83E+01
FeO	−1.20E+05	−3.62E+02	5.52E+00	−9.98E−04	4.38E−07	−6.79E−11	3.64E−15	3.04E+04	−3.63E+00
CO_2	1.18E+05	−1.79E+03	8.29E+00	−9.22E−05	4.86E−09	−1.89E−12	6.33E−16	−3.91E+04	−2.65E+01
CCN	7.95E+04	−1.34E+03	8.31E+00	−2.22E−04	1.75E−08	2.55E−12	−2.65E−16	1.02E+05	−2.26E+01
CNC	−9.03E+04	−8.31E+02	8.11E+00	−2.45E−04	5.40E−08	−6.18E−12	2.87E−16	8.45E+04	−2.10E+01
CNN	−1.82E+05	−6.73E+02	7.86E+00	−6.14E−05	−1.09E−08	4.46E−12	−2.84E−16	7.72E+04	−1.97E+01
C_2O	−6.35E+05	1.18E+03	4.88E+00	1.76E−03	−3.96E−07	3.99E−11	−1.55E−15	2.49E+04	9.81E−01
C_3	4.51E+06	−1.46E+04	2.28E+01	−8.54E−03	2.15E−06	−2.10E−10	6.35E−15	1.91E+05	−1.27E+02
O_3	−3.87E+07	1.02E+05	−8.96E+01	3.71E−02	−4.14E−06	−2.73E−10	5.25E−14	−6.52E+05	7.03E+02
N_3	2.53E+05	−2.36E+03	9.14E+00	−6.21E−04	1.32E−07	−1.48E−11	6.72E−16	6.41E+04	−3.14E+01
NCO	1.09E+05	−1.74E+03	8.66E+00	−4.05E−04	7.60E−08	−7.25E−12	3.24E−16	2.37E+04	−2.62E+01

Table 2. Thermodynamic data coefficients (b).

Particles	a_1	a_2	a_3	a_4	a_5	a_6	a_7	b_1	b_2
NO_2	7.21E+05	−3.83E+03	1.11E+01	−2.24E−03	6.55E−07	−7.61E−11	3.33E−15	2.50E+04	−4.31E+01
N_2O	3.01E+05	−2.24E+03	9.02E+00	−5.71E−04	1.20E−07	−1.34E−11	6.04E−16	2.10E+04	−3.05E+01
NCN	−1.64E+05	−7.77E+02	8.00E+00	−1.66E−04	2.98E−08	−3.12E−12	1.99E−16	6.18E+04	−2.15E+01
SiC_2	7.03E+06	−2.47E+04	3.92E+01	−2.00E−02	6.31E−06	−8.85E−10	4.53E−14	2.27E+05	−2.37E+02
SiO_2	−1.46E+05	−6.26E+02	7.96E+00	−1.85E−04	4.10E−08	−4.70E−12	2.18E−16	−3.79E+04	−2.05E+01
Si_2C	−1.25E+05	−3.41E+02	7.25E+00	−1.02E−04	2.25E−08	−2.58E−12	1.20E−16	6.61E+04	−1.15E+01
Si_2N	−2.81E+05	2.50E+02	7.09E+00	2.85E−04	−9.79E−08	1.55E−11	−8.04E−16	4.34E+04	−1.01E+01
Si_3	−1.70E+06	4.70E+03	2.62E+00	1.96E−03	−2.58E−07	6.10E−12	6.09E−16	4.28E+04	2.59E+01
AlC_2	1.47E+05	−1.36E+03	8.46E+00	−3.68E−04	7.90E−08	−8.88E−12	4.05E−16	8.71E+04	−2.13E+01
AlO_2	1.19E+05	−8.34E+02	8.31E+00	−3.54E−04	5.97E−08	4.01E−14	−3.52E−16	−2.03E+03	−1.72E+01
Al_2O	−1.17E+05	−1.78E+02	7.63E+00	−5.34E−05	1.18E−08	−1.36E−12	6.29E−17	−1.95E+04	−1.42E+01
OCCN	9.36E+05	−4.44E+03	1.37E+01	−1.65E−03	3.82E−07	−3.95E−11	1.51E−15	4.95E+04	−5.42E+01
C_2N_2	7.93E+05	−4.00E+03	1.31E+01	−8.75E−04	2.06E−07	−2.20E−11	9.97E−16	5.86E+04	−5.47E+01
CNCOCN	7.00E+05	−5.09E+03	1.95E+01	−1.30E−03	2.75E−07	−3.06E−11	1.38E−15	5.54E+04	−8.63E+01
C_3O_2	6.97E+05	−4.62E+03	1.66E+01	−1.18E−03	2.48E−07	−2.75E−11	1.24E−15	1.25E+04	−7.28E+01
C_4	9.20E+05	−1.53E+03	6.05E+00	5.25E−03	−1.78E−06	2.59E−10	−1.39E−14	1.33E+05	−7.26E+00
NO_3	−3.94E+05	−8.24E+02	1.06E+01	−2.45E−04	5.41E−08	−6.20E−12	2.87E−16	8.98E+03	−3.44E+01
N_2O_3	7.78E+05	−4.48E+03	1.67E+01	−2.06E−03	5.31E−07	−6.19E−11	2.69E−15	3.36E+04	−6.74E+01
N_2O_4	−4.58E+05	−1.60E+03	1.67E+01	−5.09E−04	1.14E−07	−1.32E−11	5.98E−16	4.31E+03	−6.57E+01
N_2O_5	−5.33E+04	−3.11E+03	2.04E+01	−9.96E−04	2.40E−07	−3.06E−11	1.50E−15	1.34E+04	−8.30E+01
Al_2C_2	1.60E+05	−1.64E+03	1.16E+01	−4.38E−04	9.37E−08	−1.05E−11	4.78E−16	7.20E+04	−3.65E+01
Al_2O_2	−1.94E+05	−4.61E+02	1.08E+01	−1.38E−04	3.04E−08	−3.50E−12	1.62E−16	−4.96E+04	−2.95E+01
Al_2O_3	−2.78E+05	−4.92E+02	1.39E+01	−1.47E−04	3.25E−08	−3.73E−12	1.73E−16	−6.79E+04	−4.38E+01
$Fe(CO)_5$	1.12E+06	−8.07E+03	3.65E+01	−2.05E−03	4.44E−07	−4.93E−11	2.24E−15	−4.86E+04	−1.75E+02
C^+	1.26E+04	−3.41E+01	2.54E+00	−2.81E−05	9.75E−09	−1.74E−12	1.25E−16	2.17E+05	4.06E+00
O^+	−2.17E+05	6.67E+02	1.70E+00	4.71E−04	−1.43E−07	2.02E−11	−9.11E−16	1.84E+05	1.01E+01
N^+	2.90E+05	−8.56E+02	3.48E+00	−5.29E−04	1.35E−07	−1.39E−11	5.05E−16	2.31E+05	−1.99E+00
Al^+	−4.18E+03	−9.95E+00	2.55E+00	−5.88E−05	3.13E−08	−7.75E−12	7.27E−16	1.09E+05	3.49E+00
Fe^+	−8.18E+05	1.93E+03	1.72E+00	3.39E−04	−9.81E−08	2.23E−11	−1.48E−15	1.29E+05	1.50E+01
Si^+	5.92E+04	−4.86E+01	2.56E+00	−3.50E−05	1.19E−08	−2.08E−12	1.47E−16	1.49E+05	5.24E+00
O_2^+	7.38E+04	−8.46E+02	4.99E+00	−1.61E−04	6.43E−08	−1.50E−11	1.58E−15	1.45E+05	−5.81E+00
NO^+	6.07E+05	−2.28E+03	6.08E+00	−6.07E−04	1.43E−07	−1.75E−11	8.94E−16	1.32E+05	−1.52E+01
N_2^+	−2.85E+06	7.06E+03	−2.88E+00	3.07E−03	−4.36E−07	2.10E−11	5.41E−16	1.34E+05	5.09E+01

Table 3. Thermodynamic data coefficients (c).

Particles	a_1	a_2	a_3	a_4	a_5	a_6	a_7	b_1	b_2
N_2O^+	−2.98E+04	−1.18E+03	8.30E+00	−2.89E−04	5.71E−08	−5.96E−12	2.84E−16	1.65E+05	−2.29E+01
CO^+	2.32E+05	−1.06E+03	4.55E+00	4.50E−04	−2.49E−07	5.27E−11	−3.29E−15	1.56E+05	−3.87E+00
CO_2^+	−1.70E+05	−8.07E+02	8.00E+00	−1.58E−04	2.57E−08	−2.40E−12	1.68E−16	1.15E+05	−2.13E+01
C_2^+	3.84E+06	−6.24E+03	2.78E+00	6.07E−03	−2.45E−06	3.88E−10	−2.19E−14	2.86E+05	7.30E−01
CN^+	−7.15E+06	1.86E+04	−1.08E+01	6.11E−03	−1.19E−06	1.18E−10	−4.80E−15	9.24E+04	1.14E+02
AlO^+	2.71E+04	−7.00E+02	5.79E+00	−6.87E−04	2.08E−07	−2.66E−11	1.28E−15	1.22E+05	−7.05E+00
Al_2O^+	−1.10E+05	−1.21E+02	7.59E+00	−3.69E−05	8.22E−09	−9.47E−13	4.41E−17	7.61E+04	−1.28E+01
$Al_2O_2^+$	−1.65E+05	−6.02E+01	1.00E+01	−1.89E−05	4.25E−09	−4.94E−13	2.31E−17	6.39E+04	−2.35E+01
C^-	4.25E+00	5.78E−04	2.50E+00	2.84E−10	−7.33E−14	9.48E−18	−4.83E−22	7.00E+04	4.88E+00
O^-	9.77E+03	7.16E+00	2.49E+00	1.97E−06	−4.30E−10	4.91E−14	−2.27E−18	1.15E+04	4.84E+00
N^-	2.40E+03	2.95E−01	2.50E+00	8.31E−08	−1.83E−11	2.10E−15	−9.75E−20	5.62E+04	5.01E+00
Fe^-	−1.24E+05	8.25E+02	1.91E+00	2.28E−04	−4.94E−08	5.59E−12	−2.57E−16	4.16E+04	1.27E+01
Si^-	−6.16E+06	1.88E+04	−1.90E+01	1.11E−02	−2.54E−06	2.70E−10	−1.11E−14	−8.31E+04	1.60E+02
Al^-	6.34E+05	−2.38E+03	5.47E+00	−1.30E−03	2.89E−07	−3.25E−11	1.47E−15	4.78E+04	−1.54E+01
N_2^-	2.17E+05	−1.28E+03	5.39E+00	−3.20E−04	7.31E−08	−8.20E−12	3.74E−16	2.42E+04	−9.01E+00
O_2^-	−5.66E+04	−2.37E+02	4.68E+00	−2.20E−05	1.71E−08	−1.76E−12	8.25E−17	−5.96E+03	−2.44E+00
CN^-	3.52E+05	−1.63E+03	5.61E+00	−3.98E−04	8.86E−08	−9.72E−12	4.43E−16	1.65E+04	−1.18E+01
AlO^-	−6.97E+04	−2.32E+02	4.67E+00	−4.27E−05	1.63E−08	−1.73E−12	8.14E−17	−3.31E+04	−2.16E+00
C_2^-	4.48E+06	−1.15E+04	1.31E+01	−1.86E−03	4.01E−08	3.71E−11	−3.34E−15	1.33E+05	−6.98E+01
AlO_2^-	−1.87E+05	−2.34E+02	7.68E+00	−7.09E−05	1.58E−08	−1.82E−12	8.45E−17	−5.59E+04	−1.77E+01
NO_3^-	−3.11E+05	−1.37E+03	1.10E+01	−4.04E−04	8.90E−08	−1.02E−11	4.72E−16	−3.36E+04	−3.88E+01
NO_2^-	1.33E+05	−1.56E+03	8.13E+00	−2.73E−04	−4.71E−08	2.83E−11	−2.35E−15	−1.72E+04	−2.23E+01

Table 4. Comparison of the concentrations of a hydrogen plasma for a temperature of the heavy species of 6000 K with a thermal imbalance of 2.

Particules	e^-	H	H^+	H_2	H_2^+	H^-
Pascal [24]	4.34E22	1.09E24	4.33E22	4.55E21	7.47E19	1.12E14
Results	4.34E22	1.07E24	4.33E22	3.57E21	6.73E19	1.08E14
Gap (%)	0	1.86	0	27.45	10.99	3.7

To validate our calculation program, we compare the concentrations of the particles of hydrogen plasma for a thermal imbalance θ of 2 for a temperature of the heavy species of 6000 K which was calculated by Pascal, with the concentrations given by our program (Table 4). We notice that the two results concord with a maximum deviation of 27.45% observed for the H_2 molecule. The differences observed can be explained by the data used. In general, we can say that our program is valid since our values concord with those of the literature.

We represent in Figures 1-5 respectively the concentration of chemical species

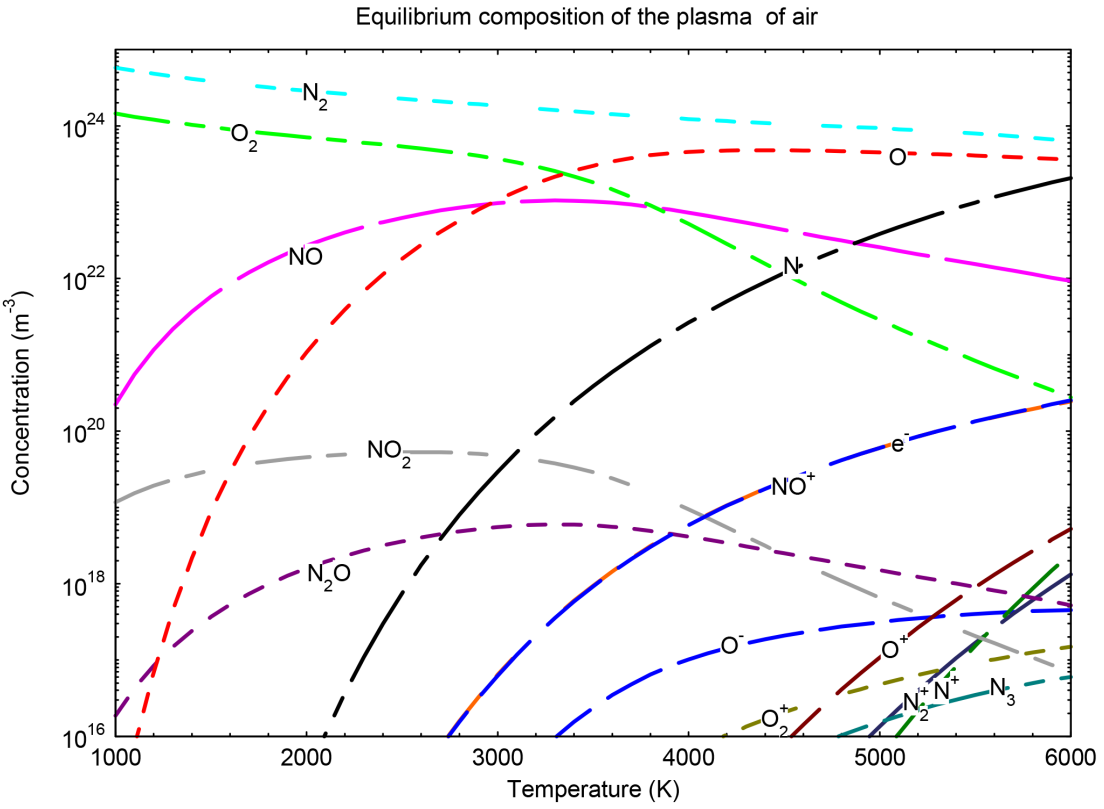

Figure 1. Equilibrium composition of the plasma of dry air at atmospheric pressure and LTE.

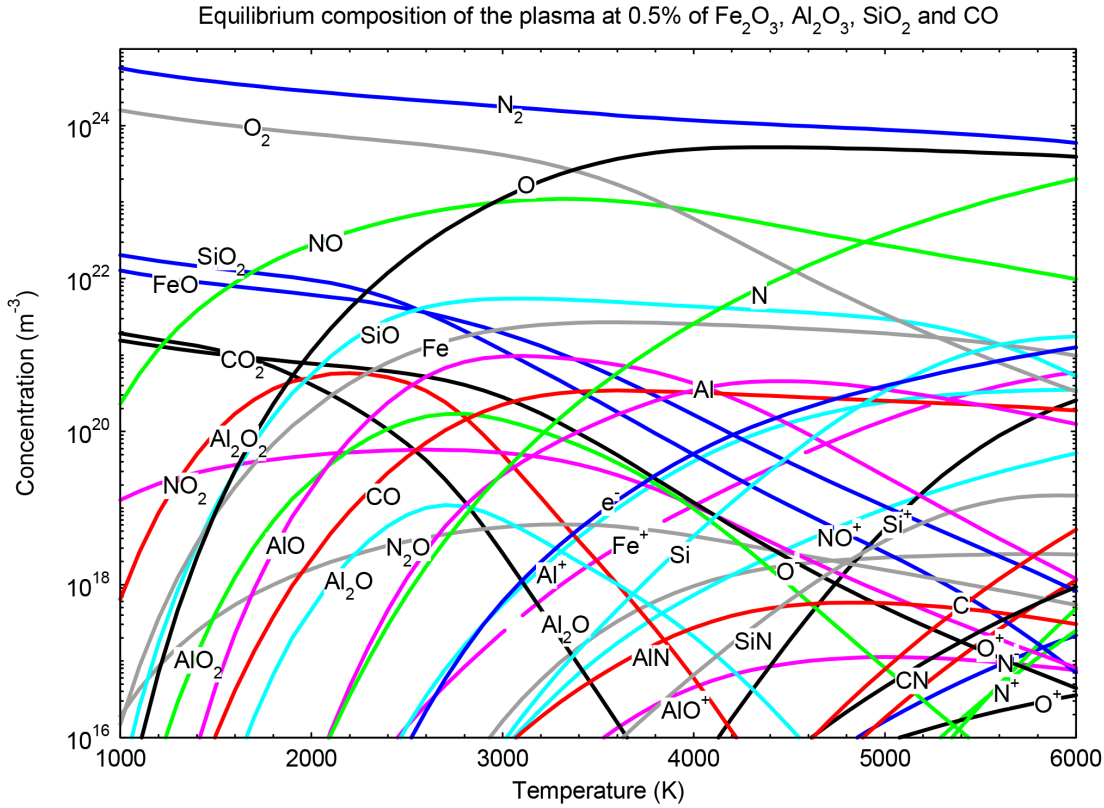

Figure 2. Concentrations of plasma mixture 99.5% of air and 0.5% of Fe_2O_3, SiO_2, Al_2O_3 and CO at atmospheric pressure and LTE.

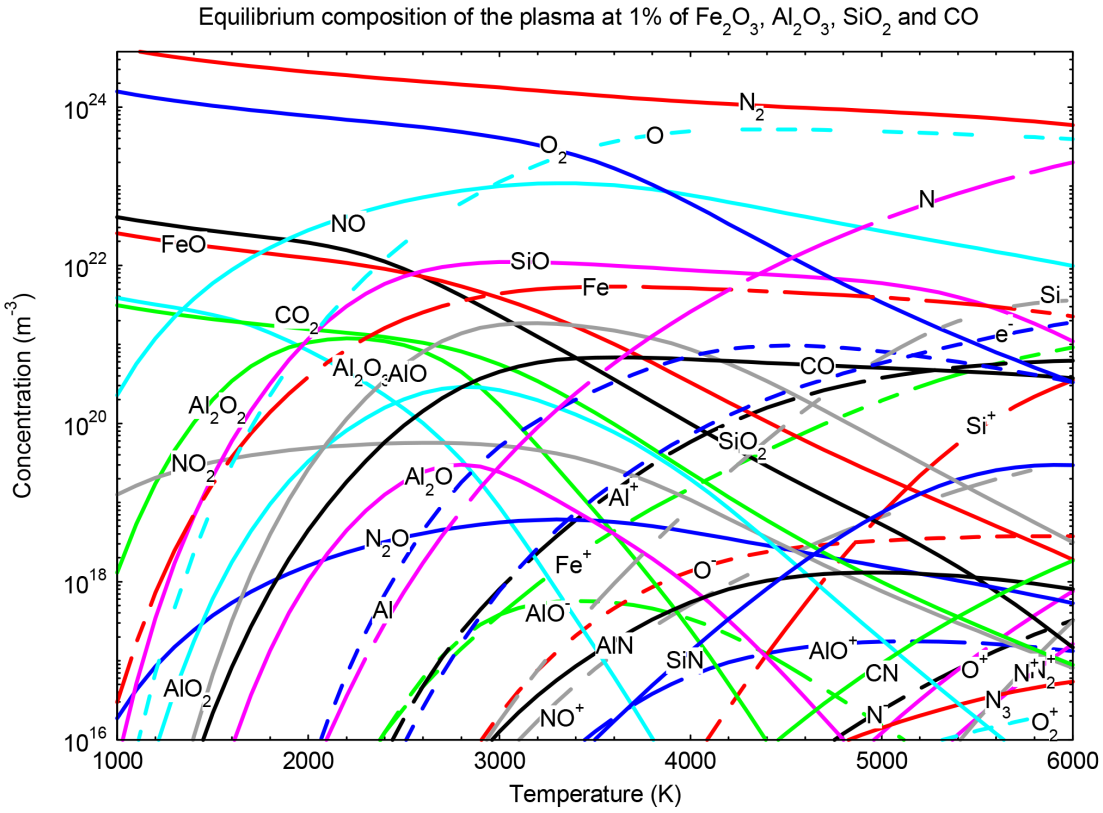

Figure 3. Concentrations of plasma mixture 99% of air and 1% of Fe_2O_3, SiO_2, Al_2O_3 and CO at atmospheric pressure and LTE.

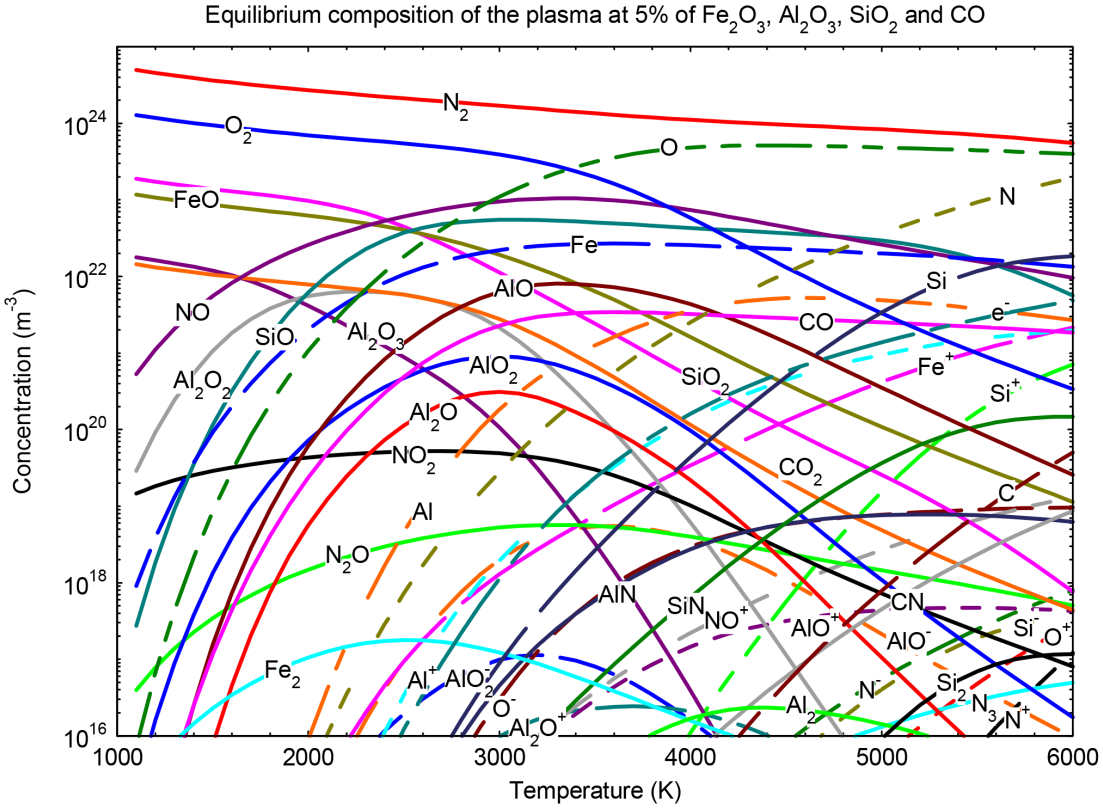

Figure 4. The concentrations of plasma mixture 95% of air and 5% of Fe_2O_3, SiO_2, Al_2O_3 and CO at atmospheric pressure and LTE.

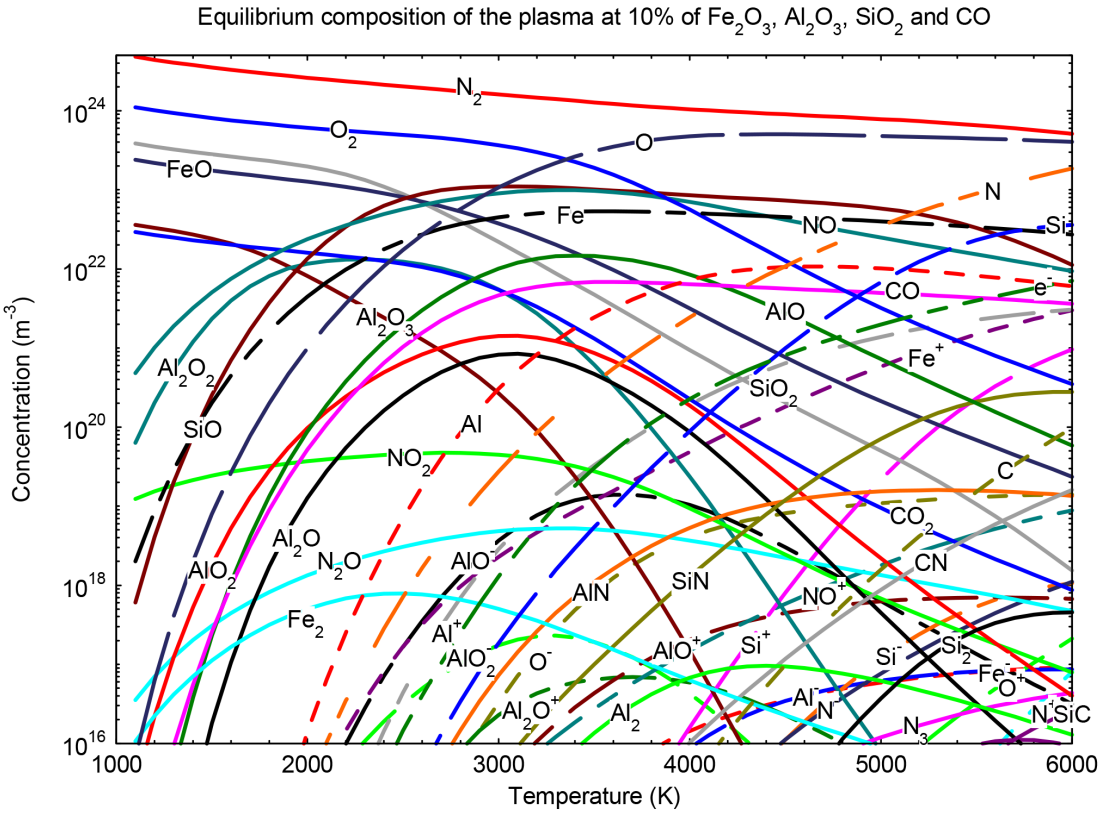

Figure 5. The concentrations of plasma mixture 90% of air and 10% of Fe_2O_3, SiO_2, Al_2O_3 and CO at atmospheric pressure and LTE.

versus temperature at atmospheric pressure and local thermodynamic equilibrium (LTE) of the plasmas formed of 100% air, 99.5% air - 0.5% impurites, 99% air - 1% impurites, 95% air - 5% impurites, 90% air - 10% impurites.

In general, we noticed that the numerical densities of the chemical species of the different plasmas evolve in a similar way in two (2) phases.

For air dry (**Figure 1**), the first phase concerns temperature less than 3000 K (T < 3000 K). This phase is mainly composed by N_2O, NO_2, N_2, O_2, and NO. The second phase concerns the temperature range of 3000 K to 6000 K (3000 K < T < 6000 K). In this interval, the main chemical species are: N_2, O_2, NO N, O, NO^+, O^+, N^+, e^-, N_2^+ and O_2^+. Densities of N_2^+, O_2^+ and O^- species appear with low concentration. In this temperature range, densities of N_2, O_2, NO, N_2O and NO_2 decrease with temperature while N, O, NO^+, O^+, N^+, e^- increase with temperature. This decrease of N_2, O_2, NO, N_2O and NO_2 is due to their low dissociation energy: O_2 dissociates to form atomic oxygen at approximately 3300 K. N_2 also dissociates to form nitrogen. Dissociation of NO leads to the formation of oxygen and nitrogen.

Electrical neutrality was rigorously established between electrons and NO^+ ions over the entire temperature range.

To estimate the effect of the percentage of Fe_2O_3, SiO_2, Al_2O_3 and CO on the equilibrium composition, we have show in **Figures 2-5** the numerical densities

of the majority chemical species. We noticed the same phases of evolution as in the case of air plasma. For temperatures less than 3000 K (T < 3000 K), most of the species were N_2, O_2, CO_2, FeO, Al_2O_2, Al_2O_3, NO, N_2O, NO_2, O, Fe, SiO, Al_2O, AlO_2, AlO, CO, and SiO_2. For temperatures most than 3000 K, he main chemical species are: N_2, O_2, NO, SiO, Si, AlO, SiO_2, Al_2O_2, CO, AlN, SiN, CN, N, O, Al, Fe, NO^+, AlO^+, Si, Al^+, Fe^+, Si^+, e^-, AlO^-, O^-, N^-, Al^- and Fe^-. N_2, O_2, CO_2, FeO, Al_2O_2, Al_2O_3, NO, N_2O, NO_2, O, Fe, SiO, Al_2O, AlO_2, AlO, CO, and SiO_2 decrease with temperature because, they dissociate to give mono-atomic species. The main reason for these dissociations at low temperatures is due their low dissociation energy. For example, Carbon dioxide dissociates into carbon monoxide at approximately 3000 K. The dissociation of Al_2O, AlO_2, Al_2O_2, and Al_2O_3 at temperatures below 3000 K led to an increase in the number density of Al and O. Moreover, SiO and SiO_2 dissociated at temperatures below 2500 K. This was the origin of the increase in the density of Si in the plasma. Moreover, FeO dissociated at temperatures below 3000 K. We noticed that polyatomic species from aerosols dissociated at approximately 3000 K or below 3000 K. In general, dissociation of polyatomic species leads to the emergence of atoms. These atoms, in turn, ionize to form ions and electrons. We also noticed that the increase in the amount of Fe_2O_3, SiO_2, Al_2O_3 and CO in the plasma led to an increase in the different species, except for nitrogen and dinitrogen. Electro neutrality is strictly established for temperatures below 3500 K between electrons, AlO^-, Al^+ and Fe^+ and beyond 3500 K, between electrons, Al^+ and Fe^+. because the ionization energy of the particle Al, Fe Si is low than those of N, C and O (Ei_{Al} = 5986 eV, Ei_{Si} = 8151 eV, Ei_{Fe} = 7902 eV, Ei_N =14.55 eV, Ei_O =13.628 eV and Ei_C =11.26 eV). So, Al^+, Fe^+, O^-, Al_2O^+, AlO_2^+, and AlO^- ions appeared between 2000 and 3000 K at low densities. Si+ ions appeared at approximately 4200 K.

To determine the influence of aerosols on the electron density of the air plasma, we compared the electron densities of the different mixtures (**Figure 6**). We observed that electron density increased with the aerosol rate of the mixture. This increase is justified by the fact that C, Si, Al, and Fe ionize at low temperatures by releasing electrons. This helps increase the electron density. Therefore, the electrical conductivity can be high at low temperatures because it depends on the electron density.

4. Conclusion

This study investigated the chemical composition of plasmas of air and aerosol mixtures in air circuit breakers at local thermodynamic equilibrium and at atmospheric pressure for temperatures of 6000 K. The calculation method used was the minimization of the Gibbs free energy. The numerical densities obtained made it possible to show the influence of aerosols on the chemical composition of the studied plasmas. The higher the percentage of aerosols is, the higher the density of the species is originating from these aerosols in the plasma. The increase in the electron density could be explained by the low ionization energies

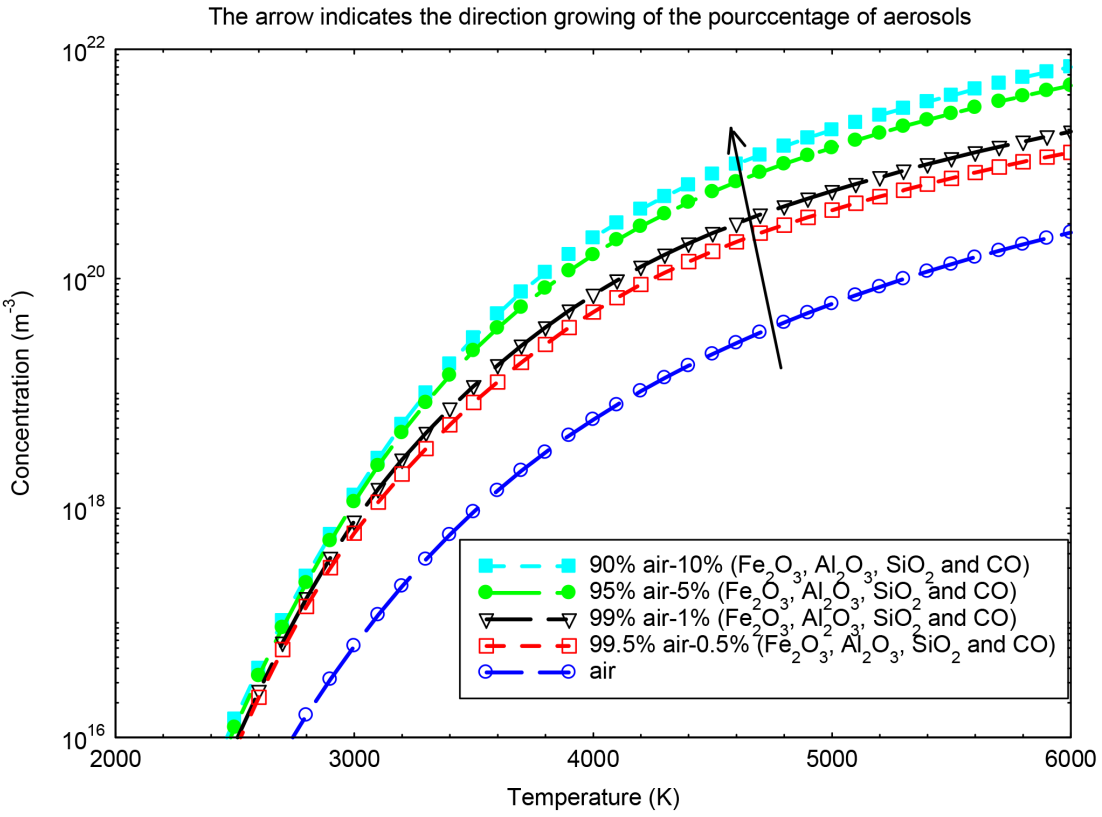

Figure 6. Evolution of the electronic density according to temperature.

of the Si, Al, and Fe species at low temperatures. This can lead to an increase in the electrical conductivity of the plasma. Therefore, the calculation of the transport coefficients is necessary to confirm this hypothesis. Thus, the slight presence of dust in the interrupting chamber of an air circuit breaker placed in a polluted atmosphere can completely modify its operation, that is, arc re-ignition and contact heating.

Conflicts of Interest

The authors declare no conflicts of interest regarding the publication of this paper.

References

[1] Note de synthèse relative à la problématique des vents de sable en provenance des deserts. Rapport de l'Institut de Veille Sanitaire (InVS), France. https://www.corse.ars.sante.fr

[2] Bouh, H.A., Benyaich, F., Bounakhla, M., Noack, Y., Tahri, M., Zahry, F. and Mater, J. (2013) Variations Saisonnières des particules atmosphériques et ses composants chimiques dans la Ville de Meknès. *Journal of Materials and Environmental Science*, **4**, 49-62.

[3] Antenne, G.J.Y. (1985) Le phénomène des brumes sèches au Sénégal, en 1984-1985. Bulletin n° 7 de l'ORSTOM et du centre de météorologie spatiale, Sénegal.

[4] Tobias, C. and Megie, C. (1980-1981) Les lithométéores au Tchad Premiers résultats

concernant la nature, la composition et l'importance des aérosols transportés par voie atmosphérique dans la région de N'Djamena (Tchad). *Office de la recherche scientifique et technique outre-mer (ORSTOM)*, **18**, 71-81.

[5] Herrmann, L., Bleich, K.E., Sterk and Stahr, K. (1997) Dépôt des poussières sur le sol en Afrique de l'Ouest: Propriétés et source des poussières et influence sur les propriés des sols et sites. Résumé de travaux, Université de Hohenheim, Institut pour la science du sol et Ecologie (310).

[6] Orange, D., Gac, J.Y. and Diallo, M.I. (1993) Constituent Composition of Harmattan Dust and Geochemical Balance of Atmospheric Deposition in Continental West Africa. *IAHS Proceedings*/*IAHS Symposium H*2*- Tracers in Hydrology*, Yokohama, 1993, 303-312.

[7] Orange, D. and Gac, J.Y. (1990) Bilan géochimique des apports atmosphériques en domaines sahélienne et soudano-guinéen d'Afrique de l'ouest (bassin s supérieurs du Sénégal et de la Gambie). *Géodynamique*, **5**, 51-65.

[8] Doumbia, E.H.T. (2012) Caractérisation physico-chimique de la pollution atmosphérique urbaine en Afrique de l'Ouest et étude de l'impact sur la santé. Thèse de doctorat de l'Université Toulouse III-Paul Sabatier, Toulouse.

[9] Michaud, V. (2009) Etude des propriétés hygroscopiques des aérosols Atmosphériques. Thèse de doctorat de l'Université Blaise Pascal, Clermont-Ferrand, N° 627.

[10] Flament, P., Deboudt, K., Cahier, H., Chatement, B. and Meriaux, X. (2011) Mineral Dust and Carbonaceous Aerosols in West Africa: Source Assessment and Haracterization. *Atmospheric Environment*, **45**, 3742-3749. https://doi.org/10.1016/j.atmosenv.2011.04.013

[11] El Hadji, T.D. (2012) Physico-Chemical Characterization of Urban Atmospheric Pollution in West Africa and Health Impact Study. Thèse de doctorat de l'Université Toulouse III-Paul Sabatier, Toulouse.

[12] Korgo, B. (2014) Caractérisation optique et microphysique des aérosols atmosphériques en zone urbaine ouest africaine: application aux calculs du forçage radiatif à Ouagadougou. Thèse de doctorat de l'Université de Ouagadougou, Ouagadougou.

[13] Nana, B. (2007) Etude de la Qualité de l'air à Ouagadougou. Rapport de campagne, Laboratoire de Physique chimique et de l'environnement (LPCE), Ouagadougou.

[14] Legrand, M. (1990) Etude des aérosols sahariens au-dessus de l'Afrique à l'aide du canal à 10 microns de METEOSAT: Visualisation, interprétation et modélisation. Thèse de doctorat de l'Université des Sciences et Techniques de Lille Flandres Artois, Lille.

[15] Malavelle, F. (2011) Effets direct et semi-direct des aérosols en Afrique de l'ouest pendant la saison sèche. Thèse de doctorat de l'Université Toulouse III Paul Sabatier (UT3 Paul Sabatier), Toulouse.

[16] Pancrati, O. (2003) Télédétection de l'aérosol désertique depuis le sol par le radiomètre infrarouge thermique multibande. Thèse de doctorat de l'Université des Sciences et Technologies de Lille, Lille.

[17] Lemaître, C. (2011) Détermination du chauffage radiatif des aérosols désertiques au-dessus de l'Afrique de l'Ouest et de leur impact sur la dynamique atmosphérique à l'aides d'observations satellitaires au cours de la campagne AMMA. Thèse de doctorat des sciences de l'environnement, Université Paris VI, Paris.

[18] André, P., Courty, M.A., Kagoné, A.K., Koalaga, Z., Kohio, N. and Zougmoré, F. (2016) Calcul de la composition chimique dans un plasma issu de mélanges de PTFE, d'air, de cuivre et de vapeur d'eau dans le cadre d'appareillages de coupure électrique à air.

[19] Cayet, S. and Dudeck, M. (1996) Equilibre chimique dans des mélanges gazeux en déséquilibre thermique. *Journal de Physique III*, *EDP Sciences*, **6**, 403-420. https://doi.org/10.1051/jp3:1996130

[20] André, P. (1995) Etude de la composition et des propriétés thermodynamiques des plasmas thermiques à l'équilibre et hors d'équilibre thermodynamique. Thèse de doctorat de l'Université Blaise PASCAL, Clermont-Ferrand II, Clermont-Ferrand.

[21] Kohio, N. (2016) Etude des propriétés thermodynamiques et des coefficients de transport des plasmas de mélange d'air et de vapeur d'eau en basses températures: Application aux disjoncteurs basse et moyenne tensions. Thèse de doctorat de l'Université Ouaga I Joseph KI-ZERBO, Burkina Faso.

[22] Case, M.W. (1998) Nist-janaf Thermochemical Tables. Fourth Édition, Part I, Al-Co. Journal Physical Chemical Reference Data. Monograph No. 9.

[23] Bendjebbar, F. andré, P., Benbakkar, M., Rochette, D., Flazi, S. and Vacher, D. (2012) Plasma Formed in Argon, Acid Nitric and Water Used in Industrial ICP Torches. *Plasma Science and Technology*, **14**, 683. https://doi.org/10.1088/1009-0630/14/8/01

[24] Bonnie, J., Gordon, S., *et al.* (2002) NASA Glenn Coefficients for Calculating Thermodynamic Properties of Individual Species. Glenn Research Center, Cleveland.

[25] NIST. http://webbook.nist.gov/chemistry

[26] André, P., Abbaoui, M. and Bessege, R. (1997) Comparison between Gibbs Free Energy Minimization and Mass Action Law for Multitemperature Plasma with Application to Nitrogen. *Plasma Chemistry and Plasma Processing*, **17**, 207-217. https://doi.org/10.1007/BF02766816

[27] Andre, P. (1996) Composition and Thermodynamic Properties of Ablated Vapours of PMMA, PA6-6, PETP, POM and PE. *Journal of Physics D*: *Applied Physics*, **29**, 1963-1972. https://doi.org/10.1088/0022-3727/29/7/033

[28] Andre, P. and Lefort, A. (1998) The Influence of Thermal Disequilibrium on a Plasma Consisting of Insulator Vapours. *Journal of Physics D*: *Applied Physics*, **31**, 717-729. https://doi.org/10.1088/0022-3727/31/6/020

[29] André, P., Ondet, J, Pellet, R. and Lefort, A. (1997) The Calculation of Monatomic Spectral Lines' Intensities and Composition in Plasma out of Thermal Equilibrium: Evaluation of Thermal Disequilibrium in ICP Torches. *Journal of Physics D*: *Applied Physics*, **30**, 2043-2055. https://doi.org/10.1088/0022-3727/30/14/012

[30] Andre, P., Ondet, J., Bouchard, G. and Lefort, A. (1999) Optical Emission Spectroscopy, Thermodynamic and Thermal Disequilibrium Aspects in an Inductively Coupled Plasma Torch. Experimental Applications to N_2-O_2 Mixtures. *Journal of Physics D*: *Applied Physics*, **32**, 920-929. https://doi.org/10.1088/0022-3727/32/8/013

[31] Faure, G. andre, P. and Lefort, A. (1999) Theoretical Calculation of Composition, Atomic and Molecular Spectral Lines in Ar-SF6 Plasma out of Thermal Equilibrium. *Journal of Physics D*: *Applied Physics*, **32**, 2376-2386. https://doi.org/10.1088/0022-3727/32/18/309

[32] André, P. and Koalaga, Z. (2010) Composition of a Thermal Plasma Formed from PTFE with Copper in Non-Oxidant Atmosphere. *High Temperature Material Processes*, **14**, 279.

[33] Kohio, N., Kagoné, A.K., Koalaga, Z. and Zougmoré, F. (2014) Composition of Air-Water Vapor Mixtures at Low Temperatures. *International Journal of Advanced Research in Science*, *Engineering and Technology*, **3**, 711-715.

[34] Rochette, D., Buissière, W. and André, P. (2004) Composition, Enthalpy and Vapo-

risation Temperature Calculation of Ag-SiO_2 Plasmas with Air in the Temperature Range from 1000 to 6000 K and for Pressure Included between 1 and 50 Bar. *Plasma Chemistry and Plasma Processing*, **24**, 475-492.
https://doi.org/10.1007/s11090-004-2280-2